Magnetic Resonance Imaging 57 (2019) 328–336

Contents lists available at ScienceDirect

Magnetic Resonance Imaging

journal homepage: www.elsevier.com/locate/mri

Original contribution

Characterizing contrast origins and noise contribution in spin-echo EPI BOLD at 3 T

Don M. Ragot, J. Jean Chen*

[a] Rotman Research Institute, Baycrest Health Sciences, Toronto, Canada
[b] Department of Medical Biophysics, University of Toronto, Canada

ARTICLE INFO

Keywords:
Spin-echo EPI
BOLD signal
Spin-echo physiological noise contribution
Spin-echo contrast-to-noise ratio
Echo-time optimization
Intravascular BOLD

ABSTRACT

In this work, we characterize contrast origins and noise contributions of spin echo (SE) EPI BOLD signal at 3 T. SE BOLD is a fMRI method of choice for imaging brain regions affected by susceptibility artifacts at lower fields, but its sensitivity remains a limiting factor for whole-brain imaging. To resolve this, the signal and noise contributions as well as TE dependence of SE EPI are characterized in this study. By integrating a two-compartment BOLD model with a physiological-thermal noise model, a new SE-BOLD signal model was introduced. The new SE-BOLD model was fit into SE-EPI fMRI data acquired during hypercapnic manipulations at various TEs, using typical fMRI voxel dimensions ($3.4 \times 3.4 \times 5\,mm^3$). Our model predicts intra- and extravascular signal and noise contributions consistent with our understanding of the SE-EPI contrast mechanism. The intravascular BOLD contribution is shown to dominate at TEs lower than tissue T_2, but the physiological noise contributions in SE-EPI signal is also shown to be lower than that of gradient-echo (GE). Furthermore, SE-EPI contrast-to-noise ratio (CNR) is not maximized at tissue T_2 as is typically assumed. To summarize, a new SE-BOLD model was proposed to characterize SE-BOLD contrast and physiological noise contribution at 3 T. Results suggests that SE-BOLD sensitivity can be improved by using shorter TEs, making it a more attractive choice for fMRI, especially in regions with susceptibility artifacts. Such optimizations could also help extend the application of SE BOLD to WM fMRI studies.

1. Introduction

Conventional BOLD functional MRI (fMRI) studies use gradient-echo (GE) EPI, which relies on T_2* contrast, driven by the static dephasing induced by magnetic-field inhomogeneities. That is, GE-BOLD contrast is caused by local magnetic field inhomogeneities resulting from susceptibility difference between oxygenated and deoxygenated blood [1–3]. While T_2* contrast is robust, it also makes GE BOLD prone to macroscopic magnetic field-inhomogeneity effects, resulting in signal dropouts and geometric distortions [4] at air/tissue interfaces and dominant BOLD activations around large veins [5–7].

In view of these limitations of GE EPI, a common alternative is using a spin-echo (SE) EPI sequence, which generates primarily T_2 contrast. The 180° pulse in SE EPI in theory refocuses static dephasing, reducing T_2* sensitivity. This suppresses the BOLD contribution from areas surrounding large veins, resulting in higher microvascular contribution and spatial specificity compared to GE techniques [8–10]. However, the loss of static-dephasing contributions to the BOLD signal results in reduced BOLD contrast compared to GE, which in turn results in lower BOLD sensitivity, limiting the current use of SE EPI in fMRI studies at lower fields.

However, an important advantage of SE BOLD even at lower field strengths is that it is a simple and powerful way to recover the majority of the MR signal lost due to strong susceptibility gradients [11,12]. This has been successfully demonstrated at 3 T, such as the orbitofrontal cortex [12] and inferior temporal lobe [13]. The success of SE EPI in these regions critical to memory and cognition demonstrate the promise of SE EPI in spite of the reduced sensitivity. Moreover, although residual T_2* weighting can be introduced through the EPI readout, SE EPI provides simple implementations and lower power deposition, and as a result as found wider applications [12–16].

The desirable attributes of SE EPI at 3 T lead us to consider whether its sensitivity can be further improved. It is increasingly recognized that optimizing the sensitivity of fMRI is contingent on an accurate understanding of signal-to-noise interactions, and more specifically, on understanding the contributions from different sources of noise, including thermal and physiological noise. These noise sources have been characterized extensively in GE BOLD using temporal signal-to-noise (tSNR)

* Corresponding author at: Rotman Research Institute, Baycrest Health Sciences, 3560 Bathurst Street, Toronto, Ontario M6A 2E1, Canada.
E-mail address: jchen@research.baycrest.org (J.J. Chen).

https://doi.org/10.1016/j.mri.2018.11.005
Received 8 August 2018; Received in revised form 6 October 2018; Accepted 11 November 2018
0730-725X/ © 2018 Elsevier Inc. All rights reserved.

and contrast-to-noise ratio (CNR) models [17–19]. More specifically, studies have shown that physiological noise dominate in GE-EPI fMRI at typical in-plane resolution of 2–3 mm [19–22]. On the other hand, similar studies of SE EPI have only been done at high fields [9,10,23,24], although 3 T is arguably the most common field strength for human fMRI research. In the absence of such empirical studies, the optimal TE for SE EPI at 3 T has been always assumed to be equal to tissue T_2 based from early simulation results [8,25,26]. However, these simulations did not consider the effect of physiological noise, which is now known to have a significant effect on BOLD sensitivity.

Multiple studies using GE [17–19] has shown that physiological noise is the primary source of BOLD signal variance at 3 T, and that its relative contribution depends on TE and voxel size [17,19]. It follows therefore that SE-EPI BOLD detectability is not necessarily optimal at tissue T_2. Although we showed recently that SE EPI is less sensitive to physiological noise compared to GE EPI [27] at 3 T, there has yet to be a full characterization of SE-BOLD noise contributions to the same extent as there is for GE BOLD. Without such a characterization, it is difficult to optimize the sensitivity of SE BOLD.

In the present study, we use a hypercapnia paradigm to induce a global BOLD signal increase, which we use to characterize the contrast origins and noise properties of SE EPI, particularly as they vary with TE. We also formulated a comprehensive SE-BOLD signal model that integrates a number of previous models. We fit our experimental data to this new model to allow it to predict intra- and extravascular signal and noise characteristics. Our results confirm similar IV and EV contributions for SE EPI at 3 T when TE is equal to tissue T_2. Moreover, we quantitatively demonstrate that the physiological noise contributions in SE EPI are lower than in GE EPI. Importantly, our results indicate that a TE equal to tissue T_2 does not lead to optimal BOLD sensitivity.

2. Theory

Our desire to better understand the SE BOLD signal and noise is driven by two factors: (i) BOLD sensitivity is not necessarily maximized at tissue T_2, as physiological noise is higher at such long TEs; (ii) for SE BOLD, the ideal means of maximizing spatial specificity is to maximize the EV contribution and minimize IV contribution, as long as the loss of sensitivity is not substantial. Our comprehensive SE-BOLD model is defined in the following subsections. This model integrates an intra- and extravascular BOLD model with a previously published physiological-thermal noise model.

2.1. Spin-echo contrast

For SE BOLD, the total fractional BOLD signal change ($\Delta S/S$) can be considered as the sum of intravascular ($\Delta S_{IV}/S$) and extravascular ($\Delta S_{EV}/S$) fractional signal changes [9]:

$$\Delta S/S = (\Delta S_{IV} + \Delta S_{EV})/S \tag{1}$$

where

$$S = V \cdot exp(-TE \cdot R_{2,blood}) + \kappa \cdot (1 - V) \cdot exp(-TE \cdot R_{2,tissue}), \tag{2}$$

$$\Delta S_{IV} = [(V + \Delta V) \cdot exp(-TE \cdot \Delta R_{2,blood}) - V] \cdot exp(-TE \cdot R_{2,blood}), \tag{3}$$

$$\Delta S_{EV} = \kappa \cdot [(1 - V - \Delta V) \cdot exp(-TE \cdot \Delta R_{2,tissue}) - (1 - V)] \cdot exp(-TE \cdot R_{2,tissue}) \tag{4}$$

In the above equations, κ is the ratio of brain and blood partition coefficient for water, V is the baseline blood volume fraction, ΔV is fractional blood volume change, $R_{2,blood}$ and $R_{2,tissue}$ are the baseline blood and tissue T_2 relaxation rates, respectively. Assuming that $|TE \cdot \Delta R_{2,tissue}| \ll 1$ and $\Delta V = 0$, the extravascular ($\Delta S_{EV}/S$) and intravascular ($\Delta S_{IV}/S$) BOLD signals can be simplified to

$$\Delta S_{EV}/S = -\kappa \cdot TE \cdot \Delta R_{2,tissue} \tag{5}$$

and

$$\Delta S_{IV}/S = -V \cdot \Delta R_{2,blood} \cdot TE \cdot exp[TE \cdot (R_{2,tissue} - R_{2,blood})] \tag{6}$$

Although changes in blood volume are not always negligible, through simulations (see Appendix A) we have confirmed that these approximations hold for our experimental conditions. Furthermore, as IV and EV contribution for SE are similar at 3 T, it is reasonable to assume that ΔV will not affect the overall relative signal. By setting $\frac{\partial(\Delta S_{IV}/S)}{\partial TE} = 0$, we derived a new parameter called maximal IV contribution (IV_{max}) to be given by

$$IV_{max} = -V \cdot \frac{\Delta R_{2,blood}}{(R_{2,blood} - R_{2,tissue}) \cdot e} \tag{7}$$

IV_{max} is the maximum IV contribution for a given baseline blood volume V and is driven solely by oxygenation changes, and for a given oxygenation change, this quantity is maximized when $TE = 1/(R_{2,blood} - R_{2,tissue})$. By combining Eqs. (6) and (7), the IV fractional signal change can be expressed as

$$\frac{\Delta S_{IV}}{S} = IV_{max} \cdot (R_{2,blood} - R_{2,tissue}) \cdot e \cdot TE \cdot exp[TE \cdot (R_{2,tissue} - R_{2,blood})]. \tag{8}$$

In brief, the behaviour of $\Delta S_{IV}/S$ depends on the baseline relaxation rate difference between blood and tissue. If $TE \cdot |R_{2,tissue} - R_{2,blood}| \ll 1$, the exponential term can be assumed to be equal to 1, leading to a linear relationship between $\Delta S_{IV}/S$ and TE. However, this condition is not true for typical SE TE range at 3 T, therefore, a linear model will not be able to fully characterize SE BOLD signal changes. Hence we used two-compartment BOLD model (Eq. (1)) to characterize SE BOLD signal. $\Delta R_{2,tissue}$ and IV_{max} can in turn be calculated by measuring $\Delta S/S$ at different TEs and fitting Eq. (1) but using approximations from Eqs. (5) and (8).

2.2. Spin-echo signal-to-noise

The total noise in the fMRI time-course can be expressed as [17].

$$\sigma = \sqrt{\sigma_0^2 + \sigma_P^2} \tag{9}$$

where σ_0 is the raw noise (which includes thermal noise and system noise) and σ_P is physiological noise. Physiological noise variance can further be broken into two components: (i) the BOLD-like, σ_B, which is TE-dependent and proportional to signal fluctuations ($\sigma_B = c_1 \Delta S_{noise}$) and (ii) the non-BOLD-like, σ_{NB}, which is TE-independent and proportional to MR signal strength ($\sigma_{NB} = c_2 S$).

The temporal SNR (tSNR) is then defined as:

$$tSNR = \frac{S}{\sqrt{\sigma_0^2 + \sigma_B^2 + \sigma_{NB}^2}} \tag{10}$$

where S is the mean image signal intensity. Eq. (10) can also be rewritten as:

$$tSNR = \frac{SNR_0}{\sqrt{1 + [((c_1 \Delta S_{noise})^2 + (c_2 S)^2)/S^2] \cdot SNR_0^2}} \tag{11}$$

where $SNR_0 = S/\sigma_0$. Following the work of Krüger and Glover [17], we further differentiate BOLD-like signal changes (ΔS_{noise}) into extravascular ($\Delta S_{EV,noise}$) and intravascular ($\Delta S_{IV,noise}$) noise. EV BOLD-like noise only describes fluctuations caused by changes in tissue relaxation rate while IV BOLD-like noise includes the effect of blood relaxation-rate fluctuations. Since we are modeling noise from the baseline BOLD signal fluctuations, we assume minimal blood volume ($\Delta V = 0$) and R_2 changes. Hence, we used Eqs. (5) and (8) to express tSNR as:

$$tSNR = \frac{SNR_0}{\sqrt{1 + [((c_{1,IV} \cdot TE \cdot exp[TE \cdot (R_{2,tissue} - R_{2,blood})] - c_{1,EV} \cdot \kappa \cdot TE))^2 + c_2^2] \cdot SNR_0^2}} \tag{12}$$

where variables including $IV_{max} \cdot (R_{2,blood} - R_{2,tissue}) \cdot e$ and $\Delta R_{2,tissue}$ from Eqs. (5) and (8) are integrated into the constants $c_{1,IV}$ and $c_{1,EV}$. By plotting tSNR as a function of TE, the constants $c_{1,IV}$, $c_{1,EV}$ and c_2 can be

determined by fitting the tSNR data to Eq. (12) and using these constants would allow us to determine λ as a function of TE:

$$\lambda^2 = ((c_{1,IV} \cdot TE \cdot exp[TE \cdot (R_{2,tissue} - R_{2,blood})] - c_{1,EV} \cdot \kappa \cdot TE))^2 + c_2^2 \quad (13)$$

This model is an extension of the work of Krüger and Glover [17], which showed λ as a measure of the relative contribution of physiological noise to the signal ($\sigma_P = \lambda S$). Using both fractional signal change and tSNR models, CNR can then be expressed as:

$$CNR = \frac{\Delta S}{\sigma} = \frac{\Delta S}{S} \cdot \frac{S}{\sigma} = \frac{\Delta S}{S} \cdot tSNR \quad (14)$$

3. Materials and methods

3.1. Participants

This study involves 7 healthy participants (4 women, age 29.3 ± 5.5 years (± SD); range 21 to 38 years). Participants were recruited from the Baycrest Participants Database, which includes individuals from Baycrest and local communities. This study was approved by the Research Ethics Board (REB) of Baycrest and experiments were performed with written consent from each participant.

3.2. Experimental paradigm

During fMRI sessions, we induced hypercapnia by administering mixtures of O_2, CO_2, and medical air using the RespirAct™ breathing circuit (Thornhill Research, Toronto, Canada), which provides interdependent targeting of end-tidal CO_2 pressure using the sequential gas delivery method [28]. Hypercapnia was induced by increasing the subject's end-tidal CO_2 ($PETCO_2$) level by ~5 mm Hg from the subject's natural baseline while maintaining end-tidal O_2. Each fMRI scan was accompanied by a block-design hypercapnia task, i.e. [48 s baseline - 96 s hypercapnia - 96 s baseline - 96 s hypercapnia - 48 s baseline].

3.3. MRI acquisition

All images were acquired using a Siemens TIM Trio 3 Tesla System (Siemens, Erlangen, Germany). The scan used 32-channel phased-array head coil reception and body-coil transmission. Anatomical images were acquired using a T_1-weighted MPRAGE 3D anatomical at an isotropic resolution of 1 mm^3 and GRAPPA acceleration factor = 2.

Functional images were acquired using SE EPI: TR = 2000 ms, 20 5-mm slices, 64 × 64 matrix, 3.4 × 3.4 × 5 mm^3 voxels, GRAPPA acceleration factor = 2, and 192 measurements (6.4 min). To reduce T_2*-induced image distortion in the SE-EPI images, we minimized the echo spacing (readout train = 35.2 ms, echo spacing = 0.55 ms, echo train length = 64). To maximize the utility of our results, we use a similar voxel size as other 3 T SE-EPI studies: Norris et al. (3 × 3 × 5 mm^3) [12], Jochimsen et al. (3.5 × 3.5 × 5 mm^3) [29], Miller et al. (3.4 × 3.4 × 3.4 mm^3) [30] and Kuroiwa et al. (3.75 × 3.75 × 5 mm^3) [31]. Images were acquired at repeated sessions, each with a different TE: 35, 45, 55, 65 and 75 ms. The TE order were not randomized. Despite not using randomizations, normalizing ΔS/S values by the $PETCO_2$ change precludes biases due to ordering.

For 5 subjects, additional customized single-slice SE-EPI scans were performed to enable measurement of the venous-blood signal in the sagittal sinus (SS) (approximating a pure intravascular signal). This customized single-slice SE EPI had the same parameters as the first functional scan except that a non-selective rectangular 180° refocusing pulse was used. Before the SS can, a sagittal maximum-projection time-of-flight image was acquired for vascular localizer and guide in positioning the axial single-slice SS scan. In standard SE EPI, only a small amount of flowing blood will experience both 90° and 180° pulses due to blood displacement resulting in reduced SE signal during fast flow. By using a non-selective 180° pulse, the displaced blood will receive both 90° and 180° pulses, minimizing signal washout caused by fast-flowing blood in the SS.

3.4. fMRI preprocessing

The fMRI data were pre-processed using FEAT package in FSL (FMRIB, Oxford University; http://fsl.fmrib.ox.ac.uk/fsl/fslwiki/FEAT). The first 2 volumes were discarded, and slice timing and motion correction, high pass filtering (< 0.005 Hz), and spatial smoothing (5 mm full-width-at-half-maximum) were performed. Lastly, fMRI images were registered to anatomical template.

3.5. Functional regions of interest (ROIs)

Grey (GM) anatomical ROIs were derived from subject-specific native space FreeSurfer tissue segmentation [32] and registered to the fMRI data separately for each TE using FSL's FLIRT command [33]. Statistical maps (*p*-values) were created by running voxel-wise two-sample *t*-test comparing hypercapnic and baseline BOLD data within each anatomical ROI and every TE. The p-value volumes were corrected for multiple comparisons using the false discovery rate (FDR) approach and GM functional masks were created using FDR of q < 0.05 for every TE. We assumed that these masks include tissue voxels that are significantly active during hypercapnia. These masks were then aligned by registration to the first TE using FSL FLIRT. Lastly, to permit a fair comparison across TEs, a new mask, namely a collection of intersection-functional ROIs, was created by only including voxels that are active for every TE. The intersection-functional ROIs were used to calculate the fractional change in BOLD signal (ΔS/S), temporal signal-to-noise ratio (tSNR) and contrast-to-noise ratio (CNR) for each TE and each subject as explained in the next section. SS ROIs were created by visual inspection, using the anatomical scans as reference for locating the approximate location of SS, and subsequently by thresholding the ΔS/S map in the SS anatomical region, based on the knowledge that large veins are associated with the highest ΔS/S responses to CO_2.

3.6. Data analysis

All simulations and data analysis were performed using in-house software written in MATLAB, 2016b (The MathWorks, Inc., Natick, MA, USA). Through simulations (see the Appendix), we verified that $\Delta S_{EV}/S$ and $\Delta S_{IV}/S$ can be simplified to Eqs. (5) and (8), respectively without loss of accuracy. Such approximations were used previously in high-field data [9,10]. We used these approximations in our models allowing us to calculate for the unknown contrast parameters ($R_{2,tissue}$ and IV_{max}) with only 5 TEs.

Within the GM anatomical ROIs, we determined the appropriate time shifts between the mean tissue BOLD signal and the $PETCO_2$ curve by finding the first local maximum peak of the cross-correlation function between the mean tissue BOLD signal and $PETCO_2$ curve. After accounting for the time shifts, we determined the mean and standard deviation of the hypercapnic and baseline BOLD signals on a voxel-wise basis and aligned all GM anatomical ROIs to a common functional space using FSL's FLIRT command. To ensure that we capture the BOLD signal at relative steady state, we computed the parameters based on the later sections of the hypercapnic and baseline blocks, as seen in Fig. 1. We used these hypercapnic and baseline BOLD data in two-sample *t*-tests to create GM intersection-functional ROIs as explained in the previous section.

Using the GM intersection-functional ROIs for all runs, ΔS/S, CNR and tSNR were calculated voxel-wise for each tissue type and for each TE:

1. ΔS/S was calculated as the difference between the mean hypercapnia and baseline BOLD signal divided by mean baseline signal;

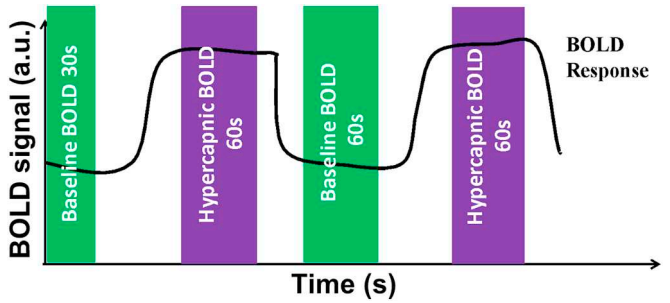

Fig. 1. Time intervals used to calculate mean and standard deviation of baseline and hypercapnic BOLD signals. Time intervals used to calculate mean and standard deviation of baseline and hypercapnic BOLD signals. The green and purple blocks represent the baseline and hypercapnic BOLD measurements, respectively, while the black line represent a hypothetical BOLD signal corresponding to this stimulation paradigm. (For interpretation of the references to colour in this figure legend, the reader is referred to the web version of this article.)

2. tSNR was calculated by dividing the mean baseline signal by the standard deviation of baseline signal;
3. CNR was calculated as the difference between the mean hypercapnia and baseline BOLD signal and divided by the standard deviation of the baseline.

Furthermore, TE-specific ΔS/S, tSNR and CNR estimates were calculated by averaging across all subjects. In the SS, the same parameters were calculated using the SS mask defined earlier. As different subjects are likely to respond differently to hypercapnic manipulation, we normalized the CNR values by the subject's response during each scan (i.e. change in end-tidal CO_2 ($\Delta PETCO_2$)). This step allowed us to minimize the biases introduced by this intersubject variability.

We calculated $R_{2,tissue}$, $R_{2,blood}$ and S_0 first by fitting an exponential-decay function to the baseline BOLD signal at different TEs using the Levenburg-Marquardt least-squares method (MATLAB's lsqnonlin function). S_0 is the extrapolated signal intensity at TE = 0 ms and was used to calculate SNR_0 for Eq. (12) [17]. To determine the IV contribution to the BOLD signal, $\Delta R_{2,tissue}$ and IV_{max} were calculated by fitting Eq. (1) (using the simplified EV- and IV-BOLD expressions from Eqs. (5) and (8)) to the measured ΔS/S values at various TEs by using the same least-squares minimization. To complete the model parameterization, we adopted the tissue κ value (0.94 for GM) from [34].

In terms of the noise parameters, to obtain λ, we first calculated the unknown noise parameters ($c_{1,IV}$, $c_{1,EV}$ and c_2) by fitting Eq. (12) to the measured tSNR values. This allowed us to estimate the relative contribution of physiological noise to the signal ($\lambda = \sigma_P/S$) using our multi-TE data. σ_0 was determined using the method described in [35].

Lastly, to ensure that our noise measurements are not biased by motion during the task blocks, we computed the framewise displacement based on MCFLIRT results.

4. Results

We show BOLD t-statistics map in grey (GM) in Fig. 2a. Voxels that are significantly active for every TE are also shown in Fig. 2b.

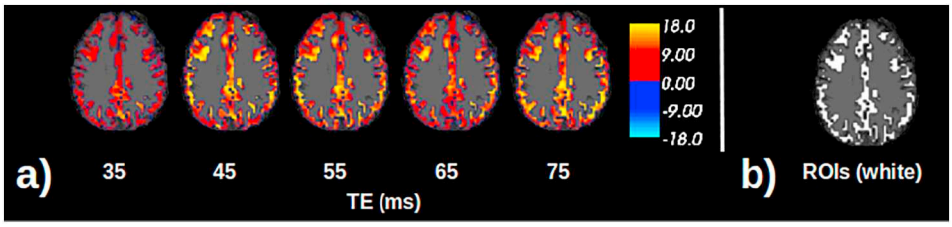

Fig. 2. BOLD activation maps from an individual subject. a) Map of t-statistics for BOLD in grey matter for every TE. The colour bar represents t statistics. (b) The final ROI only includes voxels that are significantly active for every TE (shown as a white binary mask). (For interpretation of the references to colour in this figure legend, the reader is referred to the web version of this article.)

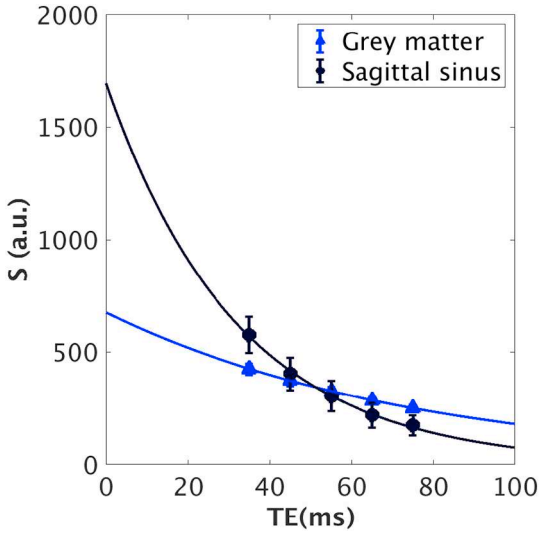

Fig. 3. Signal decay curves for grey matter and venous blood (sagittal sinus) as a function of TE. The mean BOLD signal for different subjects is measured and plotted as a function of TE. An exponential decay function is used to calculate T_2 and the curve of best fit is shown as a solid line. Error bars represent standard error from the mean.

The mean framewise displacement during hypercapnia and baseline blocks are 0.08 ± 0.03 mm and 0.07 ± 0.02 mm (± SD) respectively, showing no significant difference in head motion during hypercapnia and baseline.

The group-mean BOLD signal decay curves are shown in Fig. 3. The nonlinear fit results in calculated experimental T_2 of 75.6 ± 2.9 ms and 32.1 ± 3.8 ms (± denotes 95% confidence interval) for GM and venous blood, respectively. The calculated GM T_2 is comparable to previously calculated values from literature [36,37], and the sagittal-sinus T_2 is consistent with previous measurements at 3 T, assuming ~40% Hct and a blood oxygenation saturation of Y = 0.70 [38–40].

In Fig. 4a, we show ΔS/S plotted as a function of TE. Based on our model, our extrapolated ΔS/S value is similar to that measured by Kuroiwa et al. [31] and Miller et al. [30] at a TE of 71.3 ms and 100 ms, respectively, using a similar mild hypercapnia paradigm and voxel resolution at 3 T, shown in Table 1. Furthermore, the sagittal sinus (SS) is associated with significantly higher ΔS/S values than GM, as shown in Fig. 4b, with the highest normalized ΔS/S value being ~3%/mm Hg at TE = 75 ms.

Applying these values to Eq. (1) (and using approximations described in Eqs. (5) and (8)), the fitted $\Delta R_{2,tissue}$ values for GM is $-0.06 \pm 0.04\,s^{-1}$(± denotes 95% confidence interval). These $\Delta R_{2,tissue}$ estimates represent the EV component (as seen in Eq. (5)) and are in agreement with previously reported values by Kuroiwa et al. [31] and Jochimsen et al. [29] shown in Table 1. In the latter work, flow-crusher gradients were applied to minimize IV contribution, resulting in an estimated $\Delta R_{2,tissue}$ of $\sim -0.05\,s^{-1}$ in GM in response to hypercapnia. In another study using task-based stimulation, Jochimsen et al. [29] also modeled the IV and EV components of ΔS/S using diffusion-weighted fMRI with similar voxel resolution and calculated a

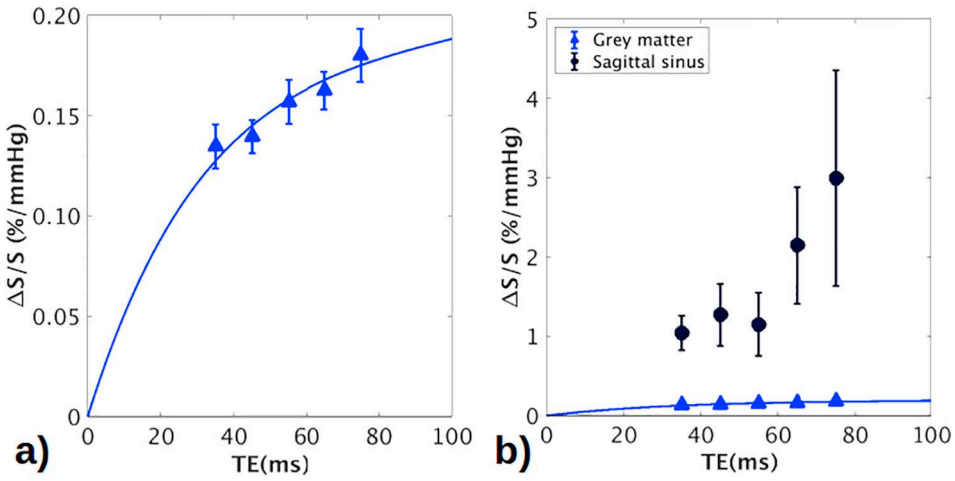

Fig. 4. Normalized ΔS/S as a function of TE. ΔS/S for different tissues are measured and averaged across all subjects. (a) Normalized ΔS/S. The solid line represents the curve of best fit using approximations from Eqs. (5) and (8). (b) The TE dependence of GM ΔS/S is overshadowed by that of the sagittal sinus. Error bars represent standard error from the group mean.

$\Delta R_{2,tissue}$ value of $-0.08\,s^{-1}$ for the EV component. Furthermore, we calculated IV_{max} value of 0.10 ± 0.04%/mm Hg (± denotes 95% confidence interval).

The estimated IV BOLD signal contribution ($\Delta S_{IV}/\Delta S$) as a function of TE is shown in Fig. 5. The solid line is the curve of best fit of Eq. (8) to the measured IV contribution values averaged across all subjects. The measured IV contribution decreases linearly with increasing TE. Furthermore, at a TE of 80 ms, our model shows good agreement with the IV contribution measured by the Jochimsen et al. [29] and Norris et al. [12], which are shown in Table 1.

In Fig. 6a, we show the measured tSNR values as a function of TE. As expected, tSNR decreases with increasing TE.

As shown in Fig. 6b, the physiological noise contribution to the signal (λ) increases with TE. At the typical TE of 75 ms, we measured physiological noise contributions (λ) of 0.60 ± 0.05% (± standard error) in the SE-EPI signal. Furthermore, we show that the SE-EPI signal exhibits lower λ values compared to GE of similar voxel size ($3.4 \times 3.4 \times 5\,mm^3$), which was characterized in Krüger and Glover [17] and displayed as '*' (Fig. 6b). Moreover, the ratio between physiological noise (σ_P) and thermal noise (σ_0) is shown in Fig. 6c. We show that physiological noise dominates across all TE in SE EPI.

Lastly, using our integrated CNR model which combines both ΔS/S and tSNR models (Eq. (14)), we determined that CNR is not in fact maximized at typical TE values used in the literature (i.e. 75–85 ms). Rather, we calculated an optimal TE of 50 ms for GM as seen in Fig. 7.

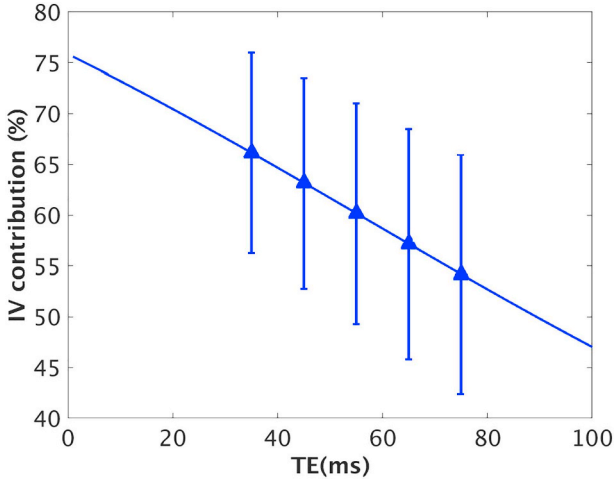

Fig. 5. The intravascular (IV) BOLD contribution as a function of TE. The solid symbols represent the IV contribution measured in different tissues averaged across all subjects, and the error bars represent standard error from the mean. The solid line represents the curve of best fit for Eq. (8).

5. Discussion

Although the use of SE EPI in BOLD fMRI has been limited at field strengths of 3 T and below due to sensitivity concerns, the advantages of SE EPI in the presence of susceptibility gradients have important implications for the study of language, memory and cognition [12,13,16,41]. Moreover, previous SE EPI studies at 3 T have shown that SE is potentially less sensitive to physiological noise compared to GE [15,27], although the noise characteristics of SE BOLD were never systematically characterized as it was for GE. Furthermore, the existing applications of SE EPI have been based on the assumption that the optimal TE is similar to tissue T_2 [11,42,43], and little attention has been paid to the role of physiological noise contributions to SE BOLD. In this context, an empirical optimization of the TE for SE BOLD, based on BOLD-like and non-BOLD-like noise behaviour is valuable.

In this study, we characterize the contrast origins and signal-to-noise (SNR) behaviour of SE-EPI signal at 3 T. We use hypercapnic challenge as a surrogate for neuronal stimulation. Hypercapnia induces a global CBF response, allowing us to study BOLD signal behaviour in

Table 1
Comparison of our measurements for SE EPI at 3 T with other literature values.

Reference	Voxel size (mm)	TE (ms)	Stimulation paradigm	ΔS/S (%)	$\Delta R_{2,tissue}(s^{-1})$	IV contribution
Present study	3.4 × 3.4 × 5	35, 45, 55, 65, 75	Mild hypercapnia ($\Delta PETCO_2$ ~ 5 mm Hg)	See Fig. 4a Based on ΔS/S model: 0.86% (TE = 71.3 ms) 0.93% (TE = 100 ms)	−0.06 ± 0.04	See Fig. 5 Based on IV model: 54.2% (TE = 75 ms) 52.7% (TE = 80 ms)
Kuroiwa et al. [31]	3.75 × 3.75 × 5	71.3	Mild hypercapnia	0.77%	~−0.05	–
Miller et al. [30]	3.4 × 3.4 × 3.4	100	Mild hypercapnia	~0.8%	–	–
Jochimsen et al. [29]	3.5 × 3.5 × 5	75	Visual stimulation	2.14%	−0.08	58%
Norris et al. [12]	3 × 3 × 5	80	Stroop colour-word matching	~2%	–	~50%

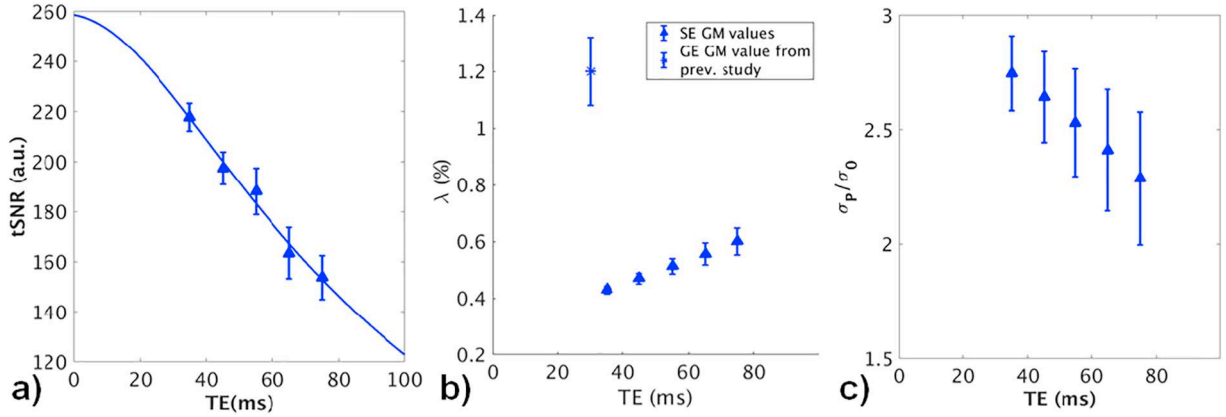

Fig. 6. TE-dependence of SE noise. (a) tSNR as a function of TE. The symbols represent the measured tSNR values averaged across all subjects and the solid line represents the curve of best fit for Eq. (12). (b) Physiological noise to signal ratio (λ) as a function of TE. Measurements are derived by averaging over all subjects and solid line represent fit to the noise model. The asterisk represents the mean λ value measured by Krüger and Glover [14] using GE. (c) Estimated ratio of physiological noise to raw noise. Error bars represent the standard error of the mean.

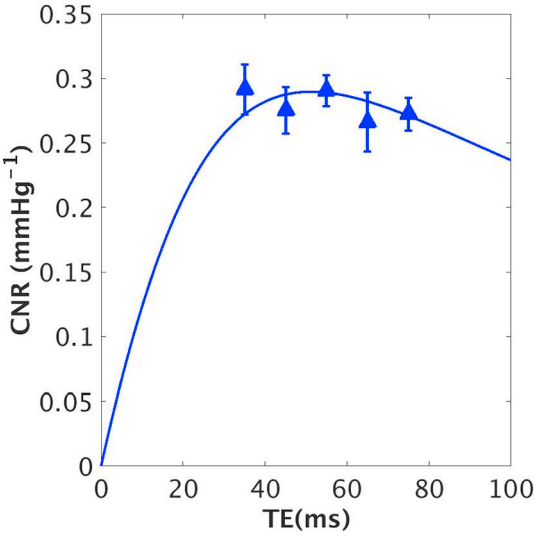

Fig. 7. Normalized CNR as a function of TE. CNR for grey matter is measured, normalized by $PETCO_2$ and averaged across all subjects. The solid line represents the CNR model based on Eq. (14) and error bars represent standard error from the mean.

different brain regions simultaneously. To that end, we developed a two-compartmental BOLD model that separates IV and EV BOLD signal contributions while incorporating a model of physiological and non-physiological noise contributions [17]. Our results show that (i) over half of SE-EPI BOLD changes come from the IV compartment at TE ≤ tissue T_2, (ii) the fractional physiological-noise contributions to the SE-EPI BOLD signal is half of that in the GE-BOLD signal at standard spin-echo and gradient-echo BOLD TEs and similar voxel volume, and (iii) the optimal TE for SE EPI can be significantly shorter than tissue T_2.

5.1. Intravascular contribution in spin-echo BOLD

Previous studies have assumed the SE-BOLD response amplitude is linearly dependent on TE [1,44,45]. This assumption is based on GE-BOLD modeling studies [1,11] in which a linear relationship between the fractional BOLD signal change (ΔS/S) and TE is commonly assumed. It was previously assumed that SE-BOLD signal changes can be completely described by ΔR_2, which combines both IV and EV BOLD effects. However, Jin et al. [9] showed empirically, at 9.4 T, that the SE BOLD signal is in fact dependent on TE in a nonlinear manner, largely attributed to the IV component [10,46,47], in agreement with model predictions. We base our model on the nonlinear ΔS/S-TE dependence described by Jin et al. [9].

In Fig. 4a, we show that at 3 T, the BOLD dependences on TE are indeed nonlinear. At the TE of 75 ms that is typically used for SE EPI at 3 T, we measured an IV contribution of ~55% for GM. Our result agrees with the measurement reported by Jochimsen et al. [29], namely a SE-EPI IV BOLD contribution of 50–60% at TE = 75 ms. We are also in agreement with the 3 T study by Norris et al. [12], who also measured a ~50% IV BOLD contribution to SE-EPI signal at a TE of 75 ms. It should be noted that both of these previous studies used similar voxel resolution as our study but used task-based stimulation and diffusion gradient-based suppression of the blood signal to isolate the IV BOLD contribution, while our measurements are solely based from modeling of multi-TE SE-EPI data. Thus, these findings appear to be robust against these methodological differences.

With this in mind, we also note that a wide range of IV contributions to SE BOLD has been reported in the broader literature, with the variability largely driven by differences in field strength and TE. The IV BOLD contribution is expected to decrease with increasing field strengths, since blood T_2 decreases more drastically than tissue T_2 at high fields. This is due to the fact that blood T_2 exhibits a quadratic dependence to magnetic field strength due to the presence of deoxyhemoglobin [38,39,46] while tissue T_2 exhibits a linear dependence as shown by Uludag et al. [26]. Furthermore, the choice of TE also affects the IV contribution; the use of longer TEs than blood T_2 will result in lower IV contribution. Simulations show that at TE equal to $T_{2,tissue}$, the IV BOLD contribution can be as high as 95% at 1.5 T and decrease to ~30% at 7 T [26] in SE. This trend is supported by other studies such as Duong et al. [10], who have measured ~70% and ~20% IV BOLD contribution at 4 T and 7 T at TE = 32 ms, respectively. At 9.4 T, Jin [9] measured ~10% IV contribution to the SE BOLD signal change at 9.4 T and a TE of 40 ms.

5.2. Physiological noise in spin-echo BOLD

While previous work by Triantafyllou et al. [20] has characterized physiological noise contribution in SE EPI as it varies with the head coil, spatial resolution and field strength, our study is the first that characterizes the TE-dependence of physiological noise contribution in SE EPI at 3 T. Our results show that when using SE EPI at 3 T, the physiological noise contribution (λ) in GM is only half that of GE at their respective typical TEs (Fig. 6b). Specifically, at a TE of 75 ms, the physiological contribution of 0.60 ± 0.05% (± standard error) is significantly lower than the 1.2 ± 0.1% (± standard error) for GE at the typical TE of 30 ms and similar voxel resolution

($3.44 \times 3.44 \times 4\,mm^3$) at 3 T, as reported by Krüger et al. [17]. This result quantitatively supports our previous observation [27] that resting-state SE EPI exhibited lower correlation with respiratory and heart-rate variability compared to GE EPI at 3 T.

We show in Fig. 6b that in SE EPI, the physiological noise contribution increases almost linearly with TE. In addition, as shown in Fig. 6c, physiological noise dominates over non-physiological noise in SE EPI at 3 T, at all TEs. At the nominal standard TE of 75 ms, the physiological-to-raw noise ratio (σ_P/σ_0) for GM is 2.3 ± 0.3. This finding is in general agreement with findings from GE at 3 T by Triantafyllou et al. [19], who measured σ_P/σ_0 of ~2 in GM at standard GE-EPI TE of 30 ms and voxel volume of 60 mm^3 (comparable to our voxel volume of ~58 mm^3). While these voxel volumes are higher than found in many experiments, we do not expect a strong voxel-size dependence in our findings, as Yacoub et al. [50] showed that σ_P/σ_0 remained constant at different voxel sizes at 7 T [50]. However, as Yacoub et al. noted, significant variations in slice thickness may introduce noise variations even if the in-plane voxel size were kept constant.

5.3. Contrast-to-noise ratio in spin-echo BOLD

A primary goal of any BOLD acquisition optimization is to maximize CNR. Using visual stimulation, Parkes et al. [15] measured a CNR of 0.9 using SE at TE = 100 ms at 3 T. This is close to the estimated CNR of 1.2 at TE = 100 ms provided by our model (Fig. 7), assuming a mean $PaCO_2$ of 5 mm Hg. Despite differences in stimulation paradigms, this is still a relevant comparison, since we have evidence through GE EPI at 3 T that a hypercapnic challenge of 5 mm Hg [51,52] elicits a BOLD response similar in amplitude to that of the visual response reported by Parkes et al. [15]. By fitting our data to the integrated SE-BOLD signal model introduced in this work, we show that SE-BOLD sensitivity is not necessarily maximized at the typically used TE, and that using shorter TEs (~50 ms) will result in similar or even higher CNR. For instance, by shortening the TE from 100 ms to 50 ms, our model predicts a ~20% increase in CNR. This is likely driven by higher tSNR at shorter TEs despite of theoretical decrease in ΔS/S at shorter TEs. The use of a shorter TE is potentially beneficial due to (i) the increased tSNR and; (ii) the reduced physiological-noise contribution, and should be investigated further in those respects.

As described earlier, the choice of the two-compartmental BOLD signal model in our integrated signal-to-noise model is driven by the observation of clear non-linearities in the SE-EPI BOLD signal dependence on TE. Such an approach allows us to selectively maximize the EV-BOLD contribution with the aim of maximizing tissue sensitivity. However, as we have shown, the IV-BOLD contribution accounts for 50% of BOLD contrast at 3 T (in the typical TE range of > 75 ms), and only declines at longer TEs. Thus, optimizing TE to eliminate the IV-BOLD contribution is not feasible at 3 T, as the corresponding loss in CNR is too prohibitive. On the other hand, using a shorter TE to maximize CNR results in higher IV-BOLD contribution and thus a reduction in tissue sensitivity. However, previous studies have shown that short-TEs can lead to higher BOLD sensitivity in regions affected by high-susceptibility and physiological noise [27,45] compared to GE. This will remain the main motivation for the adoption of SE BOLD at low-to-medium field strengths. Moreover, our framework could also help extend the application of SE BOLD to WM fMRI studies, in which T_2* weighting should be reduced while CNR should be boosted.

5.4. Caveats

In this work, we used the two-compartment BOLD and noise model, which has been used in previous SE BOLD studies [9,10,20,24,50] at 3 T and 7 T. For this model, we used the sagittal sinus (SS) data to calculate venous blood T_2, which we used for modeling blood signals in the GM. Due to the fast flow, the MR signal in the SS typically decays rapidly. We circumvent this issue by refocusing spins over a larger area using a non-slice-selective refocusing pulse. While our blood R_2 and ΔR_2 values agree with published values, the SS may not be representative of all blood, especially the blood signal in smaller vessels.

Furthermore, in this study, we examined the TE-dependence of SE-BOLD contrast and noise contribution by fitting our SE-BOLD models to multi-TE SE-EPI data. Due to scanner-hardware and scan-time constraints, we were limited to acquiring SE-EPI data at 5 TEs. One of the key assumptions in our model is that ΔS/S is equal to zero when TE = 0, and this assumption has a substantial effect on the shape of our ΔS/S curves. Thus, we would ideally aim for a wider sampling range to fully characterize the TE dependence. However, we do wish to point out that the assumption of zero BOLD sensitivity at a TE of zero is well founded in theory, as T_2 effects cannot be detected without allowing dephasing to occur. Furthermore, our CNR calculations are based on parameterizations of the tSNR and ΔS/S curves instead of the CNR data points alone. This allows us to use the tSNR and ΔS/S data (10 data points per subjects) to fit for the noise ($c_{1,IV}$, $c_{1,EV}$ and c_2) and contrast (IV_{max}) parameters, respectively, as described in the Materials and methods section.

Lastly, in this work, we focused primarily on the effect of TE on SE-EPI contrast and noise contributions at 3 T. Since we want to use the result of previous SE-EPI studies to validate our results, we opted to use similar spatial resolutions as in the existing literature for 3 T. However, the increasing practice of using smaller voxels and higher field strengths would necessitate an investigation of the effect of other fMRI acquisition parameters on SE-BOLD noise and sensitivity, such as voxel size, readout bandwidth and field strength. Furthermore, performing similar TE characterizations will be of even more interest for high-field fMRI studies, whereby higher spatial resolution can be achieved and the IV-EV contribution ratio would be very different [38,39,46].

6. Conclusions

Application of SE EPI in fMRI has been limited due to its reduced sensitivity compared to GE EPI. However, the signal-to-noise behaviour of SE BOLD has not been properly investigated outside of simulations. In this study, we developed an analytical model for CNR for SE EPI by integrating a two-compartment BOLD with a BOLD physiological noise model, parameterized by a multi-TE SE-EPI dataset. Using hypercapnia stimulation to induce global BOLD increases, and by fitting the data to our integrated model, we estimate an IV contribution of ~50% at TE equal to tissue T_2, consistent with the results of previous studies. Our model further shows that the SE-BOLD IV contribution decreases linearly with TE. Furthermore, we showed that the physiological noise contribution to the SE-EPI signal is substantially lower than to that of GE. Lastly, we showed that the optimal TE for SE EPI is substantially shorter than the recommended tissue T_2. Our work suggests that contrary to previous assumptions, there is still room for improving the sensitivity of SE EPI in the current literature, and that such improvements can make SE EPI a more attractive choice, particularly in view of the reduced sensitivity of SE to strong susceptibility gradients and physiological noise.

Acknowledgments

This research was supported by the Natural Sciences and Engineering Research Council of Canada (NSERC, DMR) and the Canadian Institutes of Health Research (CIHR, JJC).

Appendix A

To fit the two-compartment BOLD signal-and-noise model to our data, we need to use the same approximations (Eqs. (5) and (6)) as used by Jin et al. [9] for SE at 9.4 T. Jin et al. based these approximations on the following assumptions: (i) $|TE{\cdot}\Delta R_{2,tissue}| \ll 1$; (ii) $\Delta V \simeq 0$. Since all TEs used in this experiment are < 0.1 s and measured $\Delta R_{2,tissue}$ for 3 T are in the order of $-0.01\ s^{-1}$ [31,53], the first assumption is likely to hold. Regarding the second assumption, we tested how a non-zero ΔV value affect these approximations at 3 T by simulating ΔS/S vs. TE curves. We followed the following steps for our simulations

1. We estimated $\Delta R_{2,blood}$ (1/s) using the following equation [39]:

$$R_2 = 11 + 125(1 - Y)^2 \quad (A.1)$$

and Y represents venous blood oxygenation level. Faracot et al. [54] measured Y = 0.665 during hypercapnia (at a level similar to ours) and Y = 0.632 at baseline. Using these values, we calculated $\Delta R_{2,blood}$ to be $-2.9\ s^{-1}$.

2. We estimated a $R_{2,tissue}$ of $-0.07\ s^{-1}$ based on results of previous studies [29,31].
3. Next, we estimated ΔV by calculating relative change in cerebral blood volume (ΔV/V). Using similar hypercapnia paradigm as ours, Chen et al. [51] estimated a change in cerebral blood flow (ΔCBF) of 4.9 ± 0.8%/mm Hg during mild hypercapnia. We targeted a $\Delta PETCO_2$ of 5 mm Hg in our experiment so we assumed a total ΔCBF of 24.5%. Using Grubb's law [55] and α = 0.18 [51], we calculated a 4% ΔV/V for hypercapnia.
4. Lastly, since ΔV depends on cerebral blood volume, we adopted a range of V values from 2% to 5% based on the results of previous studies that reported V values of ~2% and ~5% for WM and GM respectively (56–60).

The simulation results are illustrated in Fig. A.1a. Based from our simulations, the Jin approximations (solid lines) overestimate ΔS/S. Furthermore, the fractional overestimation in ΔS/S increases as ΔV increases, as seen Fig. A.1b. However, this fractional difference in the simulated BOLD signal did not surpass 12% even at the maximum ΔV value of 0.2% (corresponds to V of 5%). Moreover, the focus of our study is investigating the relationship between TE and SE BOLD signal-to-noise properties, and the assumptions regarding the value of ΔV did not alter the dependence of ΔS/S on TE. Thus, the assumptions leading up to our model approximations do not alter the main conclusions of this study.

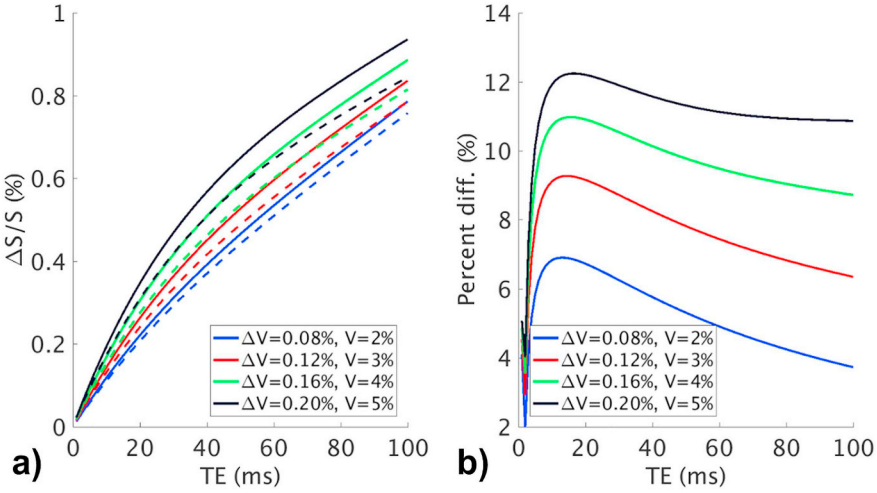

Fig. A.1. Simulated results of ΔS/S vs. TE at 3 T based on the two-compartment model. (a) Simulated ΔS/S at different V values. The dashed lines show simulation results using the full two-compartment BOLD model described in Eqs. (1)–(4) while solid lines show results based on the approximate model (given by Eqs. (5) and (6)). (b) The percent difference between the simulations results using the full and approximate two-compartment BOLD models.

References

[1] Menon RS, Ogawa S, Tank DW, Uğurbil K. Tesla gradient recalled echo characteristics of photic stimulation-induced signal changes in the human primary visual cortex. Magn Reson Med 1993;30:380–6.
[2] Ogawa S, Lee TM, Kay AR, Tank DW. Brain magnetic resonance imaging with contrast dependent on blood oxygenation. Proc Natl Acad Sci U S A 1990;87:9868–72.
[3] Ogawa S, Lee TM, Nayak AS, Glynn P. Oxygenation-sensitive contrast in magnetic resonance image of rodent brain at high magnetic fields. Magn Reson Med 1990;14:68–78.
[4] Ojemann JG, Akbudak E, Snyder AZ, McKinstry RC, Raichle ME, Conturo TE. Anatomic localization and quantitative analysis of gradient refocused echo-planar fMRI susceptibility artifacts. NeuroImage 1997;6:156–67.
[5] Duyn JH, Moonen CT, van Yperen GH, de Boer RW, Luyten PR. Inflow versus deoxyhemoglobin effects in BOLD functional MRI using gradient echoes at 1.5 T. NMR Biomed 1994;7:83–8.
[6] Frahm J, Merboldt KD, Hänicke W. Brain or vein oxygenation or flow? On signal physiology in functional MRI of human brain activation. NMR Biomed 1994;7(1–2):45–53. [Internet].
[7] Kim SG, Hendrich K, Hu X, Merkle H. Potential pitfalls of functional MRI using conventional gradient-recalled echo techniques. NMR Biomed [Internet]. 1994.
[8] Boxerman JL, Hamberg LM, Rosen BR, Weisskoff RM. MR contrast due to intravascular magnetic susceptibility perturbations. Magn Reson Med 1995;34:555–66.
[9] Jin T, Wang P, Tasker M, Zhao F, Kim S-G. Source of nonlinearity in echo-time-dependent BOLD fMRI. Magn Reson Med 2006;55:1281–90.
[10] Duong TQ, Yacoub E, Adriany G, Hu X, Ugurbil K, Kim S-G. Microvascular BOLD contribution at 4 and 7 T in the human brain: gradient-echo and spin-echo fMRI with suppression of blood effects. Magn Reson Med 2003;49:1019–27.
[11] Bandettini PA, Wong EC, Jesmanowicz A, Hinks RS, Hyde JS. Spin-echo and gradient-echo EPI of human brain activation using BOLD contrast: a comparative study at 1.5 T. NMR Biomed 1994;7:12–20.
[12] Norris DG, Zysset S, Mildner T, Wiggins CJ. An investigation of the value of spin-echo-based fMRI using a Stroop color-word matching task and EPI at 3 T. NeuroImage 2002;15:719–26.
[13] Binney RJ, Embleton KV, Jefferies E, Parker GJM, Ralph MAL. The ventral and inferolateral aspects of the anterior temporal lobe are crucial in semantic memory: evidence from a novel direct comparison of distortion-corrected fMRI, rTMS, and semantic dementia. Cereb Cortex 2010;20:2728–38.
[14] Halai AD, Welbourne SR, Embleton K, Parkes LM. A comparison of dual gradient-

echo and spin-echo fMRI of the inferior temporal lobe. Hum Brain Mapp 2014;35:4118–28.
[15] Parkes LM, Schwarzbach JV, Bouts AA, Deckers RHR, Pullens P, Kerskens CM, et al. Quantifying the spatial resolution of the gradient echo and spin echo BOLD response at 3 Tesla. Magn Reson Med 2005;54:1465–72.
[16] Visser M, Embleton KV, Jefferies E, Parker GJ, Ralph MAL. The inferior, anterior temporal lobes and semantic memory clarified: novel evidence from distortion-corrected fMRI. Neuropsychologia 2010;48:1689–96.
[17] Krüger G, Glover GH. Physiological noise in oxygenation-sensitive magnetic resonance imaging. Magn Reson Med 2001;46:631–7.
[18] Krüger G, Kastrup A, Glover GH. Neuroimaging at 1.5 T and 3.0 T: comparison of oxygenation-sensitive magnetic resonance imaging. Magn Reson Med 2001;45:595–604.
[19] Triantafyllou C, Hoge RD, Krueger G, Wiggins CJ, Potthast A, Wiggins GC, et al. Comparison of physiological noise at 1.5 T, 3 T and 7 T and optimization of fMRI acquisition parameters. NeuroImage 2005;26:243–50.
[20] Triantafyllou C, Polimeni JR, Elschot M, Wald LL. Physiological noise in gradient echo and spin echo EPI at 3 T and 7 T. Proc Int Soc Magn Reson Med 2009;17:122.
[21] Bodurka J, Ye F, Petridou N, Murphy K, Bandettini PA. Mapping the MRI voxel volume in which thermal noise matches physiological noise—implications for fMRI. NeuroImage 2007;34:542–9.
[22] Hyde JS, Biswal BB, Jesmanowicz A. High-resolution fMRI using multislice partial k-space GR-EPI with cubic voxels. Magn Reson Med 2001;46:114–25.
[23] Yacoub E, Duong TQ, Van De Moortele P-F, Lindquist M, Adriany G, Kim S-G, et al. fMRI in humans using high spatial resolutions and high magnetic fields. Magn Reson Med 2003;49:655–64.
[24] Lee SP, Silva AC, Ugurbil K, Kim SG. Diffusion-weighted spin-echo fMRI at 9.4 T: microvascular/tissue contribution to BOLD signal changes. Magn Reson Med 1999;42:919–28.
[25] Boxerman JL, Bandettini PA, Kwong KK, Baker JR, Davis TL, Rosen BR, et al. The intravascular contribution to fMRI signal change: Monte Carlo modeling and diffusion-weighted studies in vivo. Magn Reson Med 1995;34:4–10.
[26] Uludağ K, Müller-Bierl B, Uğurbil K. An integrative model for neuronal activity-induced signal changes for gradient and spin echo functional imaging. NeuroImage 2009;48:150–65.
[27] Khatamian YB, Golestani AM, Ragot DM, Chen JJ. Spin-echo resting-state functional connectivity in high-susceptibility regions: accuracy, reliability, and the impact of physiological noise. Brain Connect 2016;6:283–97.
[28] Slessarev M, Han J, Mardimae A, Prisman E, Preiss D, Volgyesi G, et al. Prospective targeting and control of end-tidal CO_2 and O_2 concentrations. J Physiol 2007;581:1207–19.
[29] Jochimsen TH, Norris DG, Mildner T, Möller HE. Quantifying the intra- and extravascular contributions to spin-echo fMRI at 3 T. Magn Reson Med 2004;52:724–32.
[30] Miller KL, Bulte DP, Devlin H, Robson MD, Wise RG, Woolrich MW, et al. Evidence for a vascular contribution to diffusion FMRI at high b value. Proc Natl Acad Sci U S A 2007;104:20967–72.
[31] Kuroiwa D, Obata T, Kawaguchi H, Autio J, Hirano M, Aoki I, et al. Signal contributions to heavily diffusion-weighted functional magnetic resonance imaging investigated with multi-SE-EPI acquisitions. NeuroImage 2014;98:258–65.
[32] Fischl B, Salat DH, Busa E, et al. Whole brain segmentation: automated labeling of neuroanatomical structures in the human brain. Neuron 2002;33:341–55.
[33] Jenkinson M, Bannister P, Brady M, Smith S. Improved optimization for the robust and accurate linear registration and motion correction of brain images. NeuroImage 2002;17:825–41.
[34] Roberts DA, Rizi R, Lenkinski RE, Leigh Jr. JS. Magnetic resonance imaging of the brain: blood partition coefficient for water: application to spin-tagging measurement of perfusion. J Magn Reson Imaging 1996;6:363–6.
[35] Wu G, Li S-J. Theoretical noise model for oxygenation-sensitive magnetic resonance imaging. Magn Reson Med 2005;53:1046–54.
[36] Stanisz GJ, Odrobina EE, Pun J, Escaravage M, Graham SJ, Bronskill MJ, et al. T1, T2 relaxation and magnetization transfer in tissue at 3 T. Magn Reson Med 2005;54:507–12.
[37] Wansapura JP, Holland SK, Dunn RS, Ball Jr. WS. NMR relaxation times in the human brain at 3.0 tesla. J Magn Reson Imaging 1999;9:531–8.
[38] Meyer ME, Yu O, Eclancher B, Grucker D, Chambron J. NMR relaxation rates and blood oxygenation level. Magn Reson Med 1995;34:234–41.
[39] Zhao JM, Clingman CS, Närväinen MJ, Kauppinen RA, van Zijl PCM. Oxygenation and hematocrit dependence of transverse relaxation rates of blood at 3 T. Magn Reson Med 2007;58:592–7.
[40] Chen JJ, Pike GB. Human whole blood T2 relaxometry at 3 Tesla. Magn Reson Med 2009;61:249–54.
[41] Pobric G, Jefferies E, Ralph MAL. Anterior temporal lobes mediate semantic representation: mimicking semantic dementia by using rTMS in normal participants. Proc Natl Acad Sci U S A 2007;104:20137–41.
[42] Constable RT, Kennan RP, Puce A, McCarthy G, Gore JC. Functional NMR imaging using fast spin echo at 1.5 T. Magn Reson Med 1994;31:686–90.
[43] Ogawa S, Menon RS, Tank DW, Kim SG, Merkle H, Ellermann JM, et al. Functional brain mapping by blood oxygenation level-dependent contrast magnetic resonance imaging. A comparison of signal characteristics with a biophysical model. Biophys J 1993;64:803–12.
[44] Stroman PW, Krause V, Malisza KL, Frankenstein UN, Tomanek B. Characterization of contrast changes in functional MRI of the human spinal cord at 1.5 T. Magn Reson Imaging 2001;19:833–8.
[45] Stroman PW, Krause V, Frankenstein UN, Malisza KL, Tomanek B. Spin-echo versus gradient-echo fMRI with short echo times. Magn Reson Imaging 2001;19:827–31.
[46] Silvennoinen MJ, Clingman CS, Golay X, Kauppinen RA, van Zijl PCM. Comparison of the dependence of blood R2 and R2* on oxygen saturation at 1.5 and 4.7 Tesla. Magn Reson Med 2003;49:47–60.
[47] Spees WM, Yablonskiy DA, Oswood MC, Ackerman JJ. Water proton MR properties of human blood at 1.5 Tesla: magnetic susceptibility, T(1), T(2), T*(2), and non-Lorentzian signal behavior. Magn Reson Med 2001;45:533–42.
[50] Yacoub E, Van De Moortele P-F, Shmuel A, Uğurbil K. Signal and noise characteristics of Hahn SE and GE BOLD fMRI at 7 T in humans. NeuroImage 2005;24:738–50.
[51] Chen JJ, Pike GB. MRI measurement of the BOLD-specific flow-volume relationship during hypercapnia and hypocapnia in humans. NeuroImage 2010;53:383–91.
[52] Ito H, Kanno I, Ibaraki M, Hatazawa J, Miura S. Changes in human cerebral blood flow and cerebral blood volume during hypercapnia and hypocapnia measured by positron emission tomography. J Cereb Blood Flow Metab 2003;23:665–70.
[53] Jochimsen TH, Ivanov D, Ott DVM, Heinke W, Turner R, Möller HE, et al. Whole-brain mapping of venous vessel size in humans using the hypercapnia-induced BOLD effect. NeuroImage 2010;51:765–74.
[54] Faraco CC, Strother MK, Siero JCW, Arteaga DF, Scott AO, Jordan LC, et al. The cumulative influence of hyperoxia and hypercapnia on blood oxygenation and R^*_2. J Cereb Blood Flow Metab 2015;35:2032–42.
[55] Grubb Jr. RL, Raichle ME, Eichling JO, Ter-Pogossian MM. The effects of changes in $PaCO_2$ on cerebral blood volume, blood flow, and vascular mean transit time. Stroke 1974;5:630–9.